Case Studies in Thermal Engineering 28 (2021) 101510

Contents lists available at ScienceDirect

Case Studies in Thermal Engineering

journal homepage: www.elsevier.com/locate/csite

The effect of nanoparticle shape on alumina/EG-water (50:50) nanofluids flow within a solar collector: Entropy and exergy investigation

Abdullah K. Alanazi [a], Yacine Khetib [b,c], Hala M. Abo-Dief [a], Muhyaddin Rawa [c,d], Goshtasp Cheraghian [e,*], Mohsen Sharifpur [f,g,**]

[a] Department of Chemistry, College of Science, Taif University, P.O. Box 11099, Taif, 21944, Saudi Arabia
[b] Mechanical Engineering Department, Faculty of Engineering, King Abdulaziz University, Jeddah, 80204, Saudi Arabia
[c] Center Excellence of Renewable Energy and Power, King Abdulaziz University, Jeddah, 80204, Saudi Arabia
[d] Department of Electrical and Computer Engineering, Faculty of Engineering, King Abdulaziz University, Jeddah, 21589, Saudi Arabia
[e] Independent Researcher, 38106, Braunschweig, Germany
[f] Department of Mechanical and Aeronautical Engineering, University of Pretoria, Pretoria, 0002, South Africa
[g] Department of Medical Research, China Medical University Hospital, China Medical University, Taichung, 404, Taiwan

ARTICLE INFO

Keywords:
Solar collector
Exergy
Entropy generation
Nanoparticle shape

ABSTRACT

In this paper, the entropy generation (E_{Gen}) and exergy of a solar collector (SC) with alumina/ethylene glycol-water (50:50) nanofluid (NFs) flow are calculated. The tubes and the absorber plate of the collector are made of copper and steel, and the results of both materials are compared. Tubes with hexagonal cross section are considered. Nanoparticles (NPs) with four different shapes of platelet, brick, blade, and cylinder are considered, and their effect is evaluated. Volume fraction (ϕ) changes in the range of 0–4%, and mass flow rate varies from 0.25 to 1 kg/s. These parameters as well as the material of collector tubes and the shape of NPs are the variables of this study and their effect on fluid frictional entropy generation ($S_{g,ff}$), thermal entropy generation ($S_{g,th}$), total entropy generation ($S_{g,tot}$), exergy output (Ex_{out}), and exergy loss (Ex_{loss}) is examined. Proposed relationships and an in-house code in MATLAB software are used for analysis. The results demonstrated that the use of copper tube leads to smaller amounts of $S_{g,ff}$, and $S_{g,tot}$ than steel tube. Besides, the Ex_{out} for cooper tubes is higher than that for steel ones. An increment in the flow rate enhances $S_{g,tot}$. Increasing the fluid mass flow rate from 0.25 to 1 kg/s increases the values of $S_{g,tot}$ 7.9 and 8.4 times for the steel and copper collectors, respectively. The addition of NPs reduces $S_{g,th}$ but enhances $S_{g,ff}$ at high values of ϕ. The addition of 4% of all shapes NPs intensifies the magnitudes of Ex_{out} and Ex_{loss}.

1. Introduction

A massive amount of greenhouse gases are produced by humans annually. Most of these gases are carbon dioxide. The combustion of fossil fuels in power plants, residential buildings, and cars is one of the most important contributors to greenhouse gas emissions [1].

* Corresponding author.
** Corresponding author. Department of Mechanical and Aeronautical Engineering, University of Pretoria, Pretoria, 0002, South Africa.
E-mail addresses: goshtasbc@gmail.com (G. Cheraghian), mohsen.sharifpur@up.ac.za (M. Sharifpur).

https://doi.org/10.1016/j.csite.2021.101510
Received 10 August 2021; Received in revised form 19 September 2021; Accepted 27 September 2021
Available online 28 September 2021

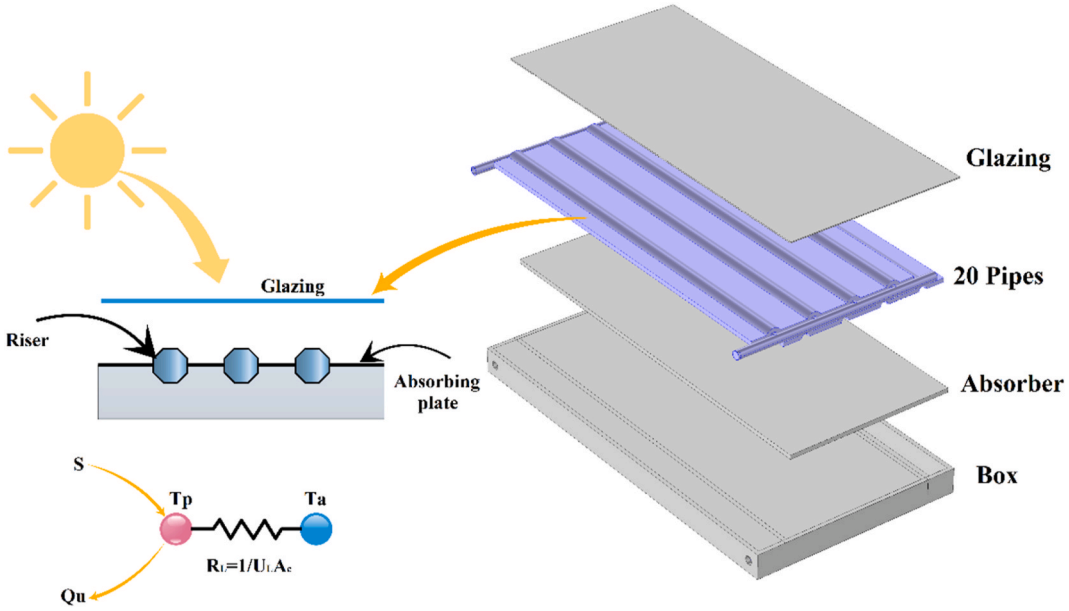

Fig. 1. Schematic of the geometry.

The consumption of fossil fuels reduces their valuable sources and also leads to the pollution of the planet. Climate change is the result of greenhouse gas emissions. Concerning climate change and the growing need for energy have led the countries to explore renewable and clean energies [2]. Wind energy, sea waves, geothermal energy, etc., are among the renewable energies available to humans, in which some countries have invested. Among these, solar energy has received more attention than other renewable energies [3–5]. One of the most widely used solar devices is SCs [6]. SCs are made in different types, and their main purpose is to transfer solar energy to the working fluid and enhance the temperature of the fluid. Flat plate collectors have become popular to provide hot water [7]. These collectors are provided in different dimensions to provide different capacities of hot water [8]. Therefore, different researchers have studied this type of collector [9–13]. Some researchers have used the numerical method and others the experimental approach to collect data [14–18]. Researchers have studied this type of collector by changing its geometry [19–21]. For instance, Kayay et al. [22] conducted an experiment to evaluate a solar water heater by changing the collector tube. Researchers have tried to resolve the problem of the low thermal conductivity of fluids [23–25]. Since Choi [26] first proposed the notion of NFs. Metal particles added to liquids improve heat conductivity; nevertheless, corrosion issues made this approach unsuitable. Many scholars have utilized nanotechnology [27–31]. NFs are made up of a mix of NPs from various materials and liquids. The thermal conductivity of NFs is greater than that of their base liquid [32,33]. Therefore, researchers have used many NFs in their works [34–36]. The use of NFs is also common in solar-based articles, and several articles have been published in this field [37–42]. For example, Aliabadi et al. [39] studied the effect of using NFs with different values of ϕ on a flat plate SC. They used an innovative geometry for their work and showed that an enhancement in the flow rate intensifies the amount of pressure drop and the heat transfer coefficient. The addition of NPs also enhances the Nusselt number.

NPs can be made and used in various shapes. Blades, platelets, cylinders, and bricks are all common forms. Because the inclusion of any of these shapes of NPs alters the quantity of thermal conductivity as well as the viscosity of NFs, these researchers set out to discover the optimal state for having the maximum heat transfer and the lowest pressure drop by experimenting with various NP [43–46]. Arani et al. [47] investigated the influence of different forms of NPs on heat transport in a mini-channel and discovered that increasing the Reynolds number increases the Nusselt number. Furthermore, using platelet-shaped NPs resulted in the smallest rise in the Nusselt number, while using brick-shaped NPs results in the largest increase.

Because NPs of various forms must be employed by various devices, they affect the thermal conductivity and viscosity of the fluid. Due to the importance of solar energy on the one hand and the importance of using NPs with different shapes, on the other hand, the impact of NPs with different shapes of blade, platelet, brick, and cylinder on a flat plate collector is studied. This study is done by using available relations. Also, since the hexagonal cross-section can transfer more heat than the circle one, tubes with hexagonal cross-section are used to measure their effect on heat transfer in the collector. Two metals, steel, and copper are employed to study the collector, and the results are compared. Finally, the values of fluid outlet temperature from the collector, the Nusselt number, and heat transfer coefficient are studied by changing the value of ϕ for different shapes of NPs when the flow rate changes from 0.25 to 1 kg/s. The use of hexagonal tubes in the collector as well as the study of the effect of nanoparticle shape and collector material on entropy and exergy was considered as the innovation of the present work.

2. Analysis of the second law of thermodynamics

Fig. 1 depicts a schematic of the present geometry.

The equations are presented below, assuming that the flow of the nanofluid is homogeneous and incompressible for the steady state, regardless of the volumetric forces [49,50]. The general relation for $S_{g,tot}$ can be written as follows [51]:

$$\dot{S}_{gen}\frac{\dot{W}_{lost}}{T_a}=\frac{\dot{E}_d+\dot{E}_l}{T_a} \tag{1}$$

where $\dot{W}_{lost}$ is the amount of lost work, $\dot{E}_l$ is the amount of leakage exergy and $\dot{E}_d$ is the amount of exergy destruction.

The amount of exergy destruction can be obtained using the following equation [52–54]:

$$\dot{E}_d=\dot{E}_{d,\Delta T_s}+\dot{E}_{d,\Delta P}+\dot{E}_{d,\Delta T_f} \tag{2}$$

where $\dot{E}_{d,\Delta T_s}$ is the exergy destruction due to the temperature difference between the sun and the absorber plate and can be written as follows:

$$\dot{E}_{d,\Delta T_s}=\eta_o G_t A_c T_a\left(\frac{1}{T_P}-\frac{1}{T_s}\right) \tag{3}$$

$\dot{E}_{d,\Delta P}$ is the exergy destruction due to the pressure drop in the SC, which is expressed as follows:

$$\dot{E}_{d,\Delta P}=\frac{\dot{m}\Delta P}{\rho}\frac{T_a\ln\left(\frac{T_{out}}{T_a}\right)}{(T_{out}-T_{in})} \tag{4}$$

$\dot{E}_{d,\Delta T_f}$ is the exergy destruction due to the NFs flow and the temperature difference between the NFs and the adsorbent plate:

$$\dot{E}_{d,\Delta T_f}=\dot{m}C_P T_a\left(\ln\left(\frac{T_{out}}{T_a}\right)-\frac{(T_{out}-T_{in})}{T_P}\right) \tag{5}$$

To obtain exergy values, it is first necessary to specify the T_P. To determine T_P, the first law of thermodynamics can be written by considering a control volume around the SC:

$$\dot{E}_{st}=\dot{E}_{in}-\dot{E}_{out}+\dot{E}_{gen} \tag{6}$$

where $\dot{E}_{st}$ is the energy absorbed by the collector, $\dot{E}_{in}$ is the energy input to the collector, $\dot{E}_{out}$ is the energy output from the collector, and $\dot{E}_{gen}$ is the energy generated in the collector. The above equation can be written as follows:

$$Q_u=A_c[\eta_o G_t-U_L(T_P-T_a)] \tag{7}$$

where Q_u is the amount of heat received by the collector, A_c is the collector area, η_o is the optical efficiency of the glass coating, G_t is the amount of input radiation on the glass plate, T_a is ambient temperature, and U_L is the overall heat transfer coefficient. This coefficient can be calculated as follows:

$$U_L=U_t+U_b+U_e \tag{8}$$

where the index t is the heat transfer from top, b is the heat transfer from bottom, and e is the heat transfer from the collector edges. The following equation can be used to calculate U_t [48]:

$$U_t=\frac{1}{\frac{N_g}{\frac{C}{T_P}\left[\frac{T_P-T_a}{N_g+\tau}\right]^{0.33}}+\frac{1}{h_W}}+\frac{\sigma\left(T_P^2+T_a^2\right)(T_P+T_a)}{\frac{1}{\varepsilon_P+0.05N_g(1-\varepsilon_P)}+\frac{2N_g+\tau-1}{\varepsilon_g}-N_g} \tag{9}$$

where N_g is equal to 1, which indicates the number of cover glasses. σ is the Stephan Boltzmann constant, ε is the collector absorption coefficient and h_W is the heat transfer coefficient of wind. The constants τ and C are obtained from the following equations:

$$\tau=\left(1-0.04h_W+0.0005h_W^2\right)\left(1+0.091N_g\right) \tag{10}$$

$$C=365.9\left(1-0.00883\beta+0.0001298\beta^2\right) \tag{11}$$

where β is the collector slope. The value of heat transfer coefficient of wind can also be obtained using the following equation [48]:

$$h_W=\frac{8.6\ V_w^{0.6}}{L^{0.4}} \tag{12}$$

Table 1
Constants for the SC [48].

Collector parameter	
β	35°
δ_c	2.5 *mm*
η_o	0.84
W	25 *cm*
n	5
L	15 *m*
D_i	2.5 *mm*
D_o	3 *mm*
T_s	4350 *K*
t_b	2 *cm*
t_e	1 *cm*
ε_p	0.92
ε_g	0.88
Solar radiation on solar collector $(\dot{q})$	1000 W/m^2
T_a	298 *K*
T_{in}	298 *K*
V_W	3 *m/s*

Table 2
Values of constants for different shapes of Al_2O_3 NPs [57].

	C_k	A_1	A_2
Platelets	2.61	37.1	612.6
Blades	2.74	14.6	123.3
Cylinders	3.95	13.5	904.4
Bricks	3.37	1.9	471.4

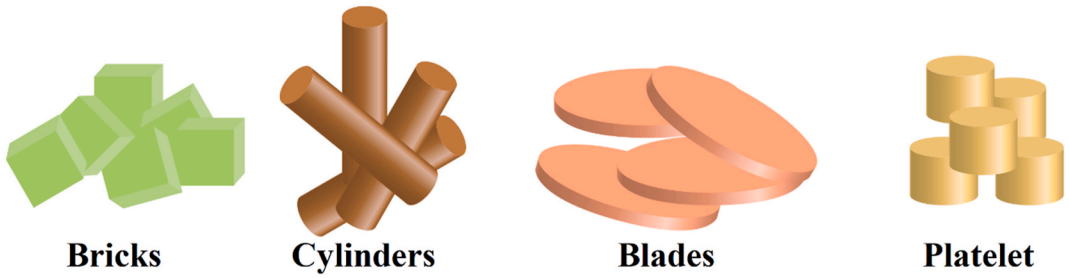

Fig. 2. Schematic of the shape of NPs.

Table 3
Thermophysical properties of alumina nanometer NPs and ethylene glycol/water 50/50 [57].

Property	C_P (J /kg.K)	k (W /m.K)	ρ(kg /m^3)	μ(kg /m.s)
Water/EG 50/50	3300	0.3799	1067.5	0.00339
AlOOH	618.3	30	3050	–

where V_w indicates wind velocity, and L is the collector length. The heat loss of the collector bottom and edges is obtained as follows:

$$U_b = \frac{1}{\frac{t_b}{k_b} + \frac{1}{h_{b,a}}} \tag{13}$$

$$U_e = \frac{1}{\frac{t_e}{k_e} + \frac{1}{h_{e,a}}} \frac{A_e}{A_c} \tag{14}$$

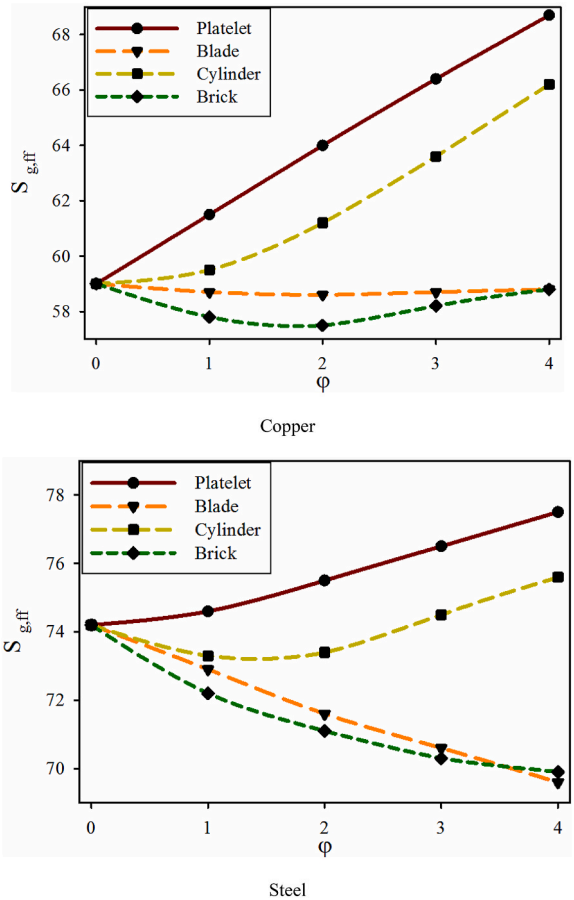

Fig. 3. The variations of $S_{g,ff}$ for different shapes and volume fractions of NPs and collector tubes made of copper and steel.

where t_b is the thickness of the insulation and k_b is the thermal conductivity of the insulation. The values of $h_{e,a}$ and $h_{b,a}$, which refer to the heat transfer coefficient around the collector edges and bottom, are equal to 5 W/m^{2}K [48].

The following is the relation of T_P. To determine U_L, it is necessary to specify the value of T_P. The value of U_L is calculated then after making the initial guess.

$$T_P = T_{in} + \frac{Q_u}{A_c F_R U_L}(1 - F_R) \tag{15}$$

By performing consecutive solutions in different loops, the final value for the above equation is reached. The convergence criterion is 10^{-5}.

F_R is related to heat removal coefficient, which is expressed as follows:

$$F_R = \frac{\dot{m} C_{p,nf}}{A_c U_L}\left[1 - exp\left(-\frac{U_L F' A_c}{\dot{m} C_{p,nf}}\right)\right] \tag{16}$$

The collector efficiency F' is calculated as follows [48]:

$$F' = \frac{\frac{1}{U_L}}{W\left[\frac{1}{U_L[D+(W-D)F]} + \frac{1}{\pi D_i h_{fi}}\right]} \tag{17}$$

where W and D indicate the distance between the tubes and the outer diameter, respectively. Index i refers to the inner diameter. The standard fin factor F is also specified as follows:

$$F = \frac{tanh[m(W-D)/2]}{m(W-D)/2} \tag{18}$$

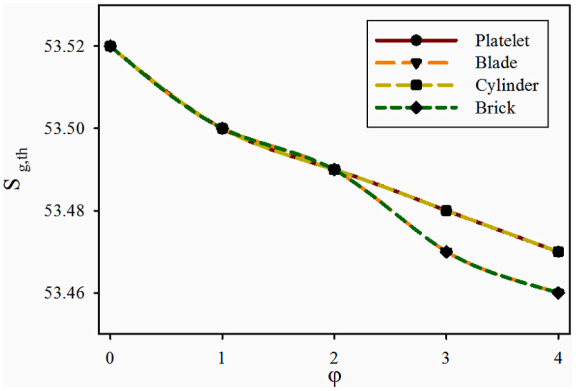

Copper

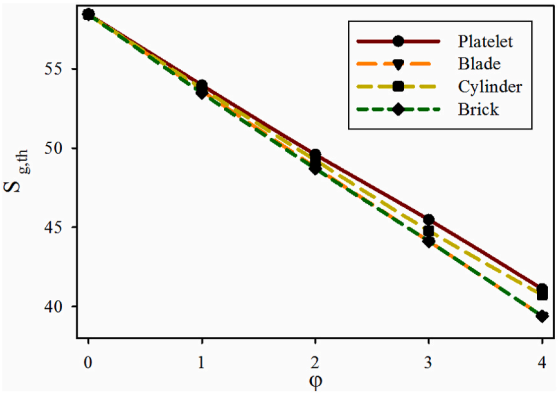

Steel

Fig. 4. $S_{g,th}$ for the blade, brick, platelet, and cylinder-shaped NPs with different values of ϕ for copper and steel collectors.

$$m = \sqrt{\frac{U_L}{k_c \delta_c}} \tag{19}$$

where k_c indicates the thermal conductivity and δ_c is the thickness of the adsorbent plate. By estimating F' and having T_P, the value of exergy can be calculated.

The amount of Leakage exergy is expressed as follows:

$$\dot{E}_l = U_L A_c (T_P - T_a)\left(1 - \frac{T_a}{T_P}\right) \tag{20}$$

Finally, the production of total entropy may be represented as follows:

$$\dot{S}_{g,tot} = \underbrace{\eta_o G_t A_c \left(\frac{1}{T_P} - \frac{1}{T_s}\right) + \dot{m} C_P \left(\ln\left(\frac{T_{out}}{T_a}\right) - \frac{(T_{out} - T_{in})}{T_P}\right) + U_L A_c \left(1 - \frac{T_a}{T_P}\right)\left(\frac{T_P}{T_a} - 1\right)}_{\dot{S}_{g,th}} + \underbrace{\frac{\dot{m}\Delta P}{\rho_{nf}} \frac{\ln\left(\frac{T_{out}}{T_a}\right)}{(T_{out} - T_{in})}}_{\dot{S}_{g,ff}} \tag{21}$$

where $\dot{m}$ is the mass flow rate, ΔP is the pressure drop, and T_s is the apparent solar temperature. The following equation may also be used to calculate the amount of pressure drop [49]:

$$\Delta P = P_1 - P_2 = \rho_{nf} g (L_r \sin\beta + h_L) \tag{22}$$

where $L_r \sin\beta$ is the vertical distance between the output and input of the collector and h_LL is the sum of the head loss in the collector. The total value of the head losses, including the major and minor head losses for the collector parallel risers, can be obtained from the following equation [55].:

$$h_{l,major} = h_{l,riser1} = h_{l,riser2} = \ldots = h_{l,riser\ n} \tag{23}$$

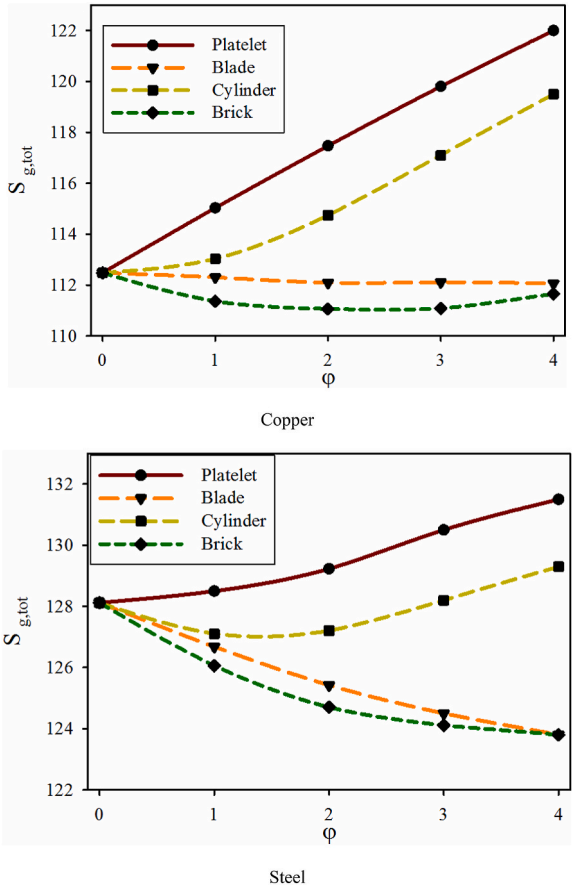

Fig. 5. $S_{g,tot}$ for the blade, brick, platelet, and cylinder-shaped NPs with different values of ϕ for copper and steel collectors.

The total head loss is:

$$h_L = h_{l,major} + h_{l,minor} = \frac{8\dot{m}_r^2}{\rho^2 g \pi^2 D_i^2}\left(f\frac{L_r}{D_i} + \sum_{i=1}^{n} K_L\right) \tag{24}$$

Finally, the equations used for exergy output and exergy loss are expressed as follows [56]:

$$\mathrm{Ex_{out}} = \dot{m}C_{p,nf}\left[(\mathrm{T_{out}} - T_a) - T_a \ln\left(\mathrm{T_{out}}/T_a\right)\right] \tag{25}$$

$$\mathrm{Ex_{loss}} = \dot{m}C_{p,nf}\left[T_a \ln\left(\mathrm{T_{out}}/\mathrm{T_{in}}\right)\right] \tag{26}$$

To determine the temperature of the fluid at the outflow, use the temperature of the adsorbent plate:

$$T_{out} = T_{in} + \frac{Q_u}{\dot{m}C_{p,nf}} \tag{27}$$

All constants introduced in the above equations are given in Table 1.

3. NFs properties

Boehmite alumina (AlOOH) NPs and ethylene glycol-water (50:50) are used for NFs preparation. The relations expressing viscosity and thermal conductivity of NFs, according to Timofeeva et al. [57] are expressed as follows:

$$\frac{\mu_f}{\mu_{bf}} = 1 + A_1\phi + A_2\phi^2 \tag{28}$$

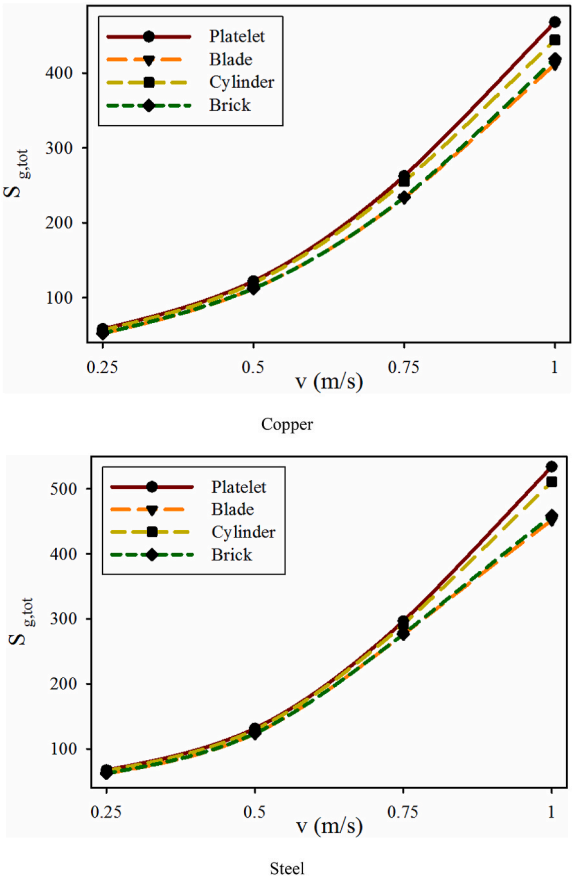

Fig. 6. $S_{g,tot}$ for the blade, brick, platelet, and cylinder-shaped NPs and different flow rates for copper and steel collectors when $\phi = 4\%$.

$$\frac{k_f}{k_{bf}} = 1 + C_k \phi \tag{29}$$

where the constant values of C_k, A_1 and A_2 are dependent on the shape of NPs, which are presented in Table 2.

The density and specific heat capacity of the NFs can also be extracted as follows, respectively.

$$\rho_f = \phi \rho_p + (1-\phi)\rho_{bf} \tag{30}$$

$$c_{p,f} = \frac{(1-\phi)(\rho c_p)_{bf} + \phi(\rho c_p)_p}{\rho_f} \tag{31}$$

where the index p represents NPs, and the index bf refers to the fluid. Fig. 2 shows a schematic of the shape of NPs.

The properties of water/ethylene glycol 50/50 and boehmite alumina NPs are given in Table 3.

4. Results and discussion

In Fig. 3, the amount of $S_{g,ff}$ for different volume fractions of blade, brick, platelet, and cylinder NPs and the collector made of copper and steel. The trend of $S_{g,ff}$ for both types of tubes is the same. In the copper tube, cylinder- and platelet-shaped NPs increase the $S_{g,ff}$ by enhancing the ϕ. Whereas the other two NPs initially reduce and then increase the $S_{g,ff}$ as ϕ is enhanced. The $S_{g,ff}$ decreases and then increases for cylinder-shaped NPs in the steel tube. However, the $S_{g,ff}$ has a descending trend for the blade NPs. The maximum value of $S_{g,ff}$ occurs when $\phi = 4\%$ for platelet-shaped NPs in both tubes. The minimum value of $S_{g,ff}$ corresponds to brick-shaped NPs when $\phi = 2\%$ and blade-shaped NPs when $\phi = 4\%$ for copper and steel tubes, respectively.

Fig. 4 shows $S_{g,th}$ for the blade, brick, platelet, and cylinder-shaped NPs with different values of ϕ for copper and steel collectors. In general, adding NPs to water/ethylene glycol reduces the amount of $S_{g,th}$ in the collector. This can be seen for both tubes. Cylinder and platelet-shaped NPs lead to a less reduction in $S_{g,th}$, while brick and blade-shaped ones result in a higher reduction of $S_{g,th}$ for both tubes. Adding all types of NPs reduces the amount of $S_{g,th}$. It can also be seen that the copper tube has less $S_{g,th}$ than the steel one. However, in steel tube, adding NPs is more effective than the copper tube and reduce $S_{g,th}$ by about 20 W/K when $\phi = 4\%$.

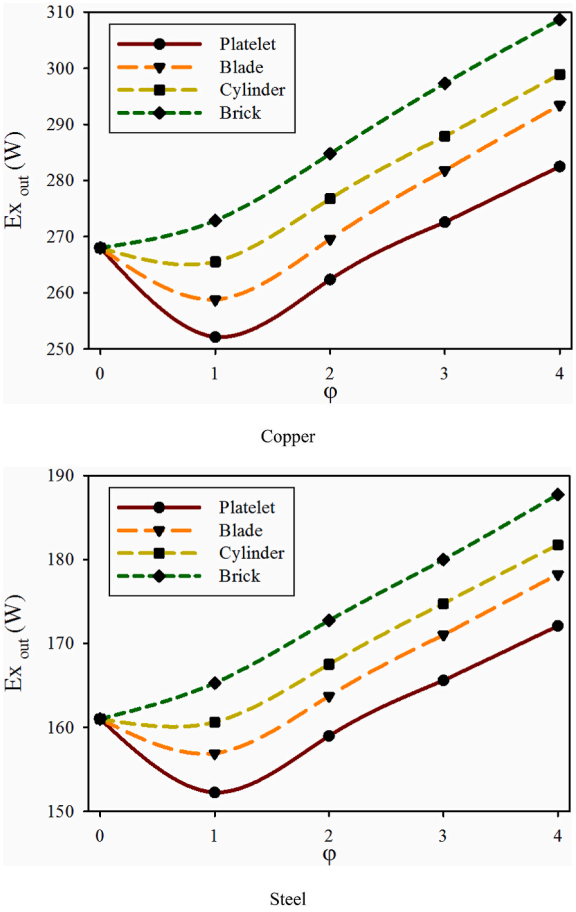

Fig. 7. The amounts of Ex_{out} for the blade, brick, platelet, and cylinder-shaped NPs with different values of ϕ for copper and steel collectors.

In Fig. 5, $S_{g,tot}$ is plotted for the blade, brick, platelet, and cylinder-shaped NPs with different values of ϕ for copper and steel collectors. It can be seen that the amount of $S_{g,tot}$ is enhanced with the addition of platelet and cylinder-shaped NPs. The addition of blade-shaped NPs leads to a little change in $S_{g,tot}$, while adding brick-shaped NPs reduces and then enhances the amount of $S_{g,tot}$. The minimum value of $S_{g,tot}$ corresponds to cooper tube for brick-shaped NPs with $\phi = 2$ and 3%. In steel tubes, the addition of platelet-shaped NPs increases $S_{g,tot}$. But for the other shapes of NPs, adding a certain amount of NPs reduces $S_{g,tot}$. For cylinder-shaped NPs, adding more NPs enhances $S_{g,tot}$, while for blade and brick-shaped ones, the $S_{g,tot}$ is reduced. The minimum value of $S_{g,tot}$ corresponds to blade-shaped NPs with $\phi = 4\%$. In general, $S_{g,tot}$ in the copper tube is less than that in steel tube, which is due to the higher thermal conductivity of copper tube.

Fig. 6 shows $S_{g,tot}$ for the blade, brick, platelet, and cylinder-shaped NPs and different flow rates for copper and steel collectors when $\phi = 4\%$. In both types of tubes, an increment in the NFs flow rate from 0.25 to 1 kg/s enhances the amount of $S_{g,tot}$. Increasing the velocity intensifies $S_{g,ff}$ and thus enhances $S_{g,tot}$. Platelet-shaped NPs have the maximum amount of $S_{g,tot}$ at all flow rates for both tubes, while blade-shaped NPs have the minimum value of $S_{g,tot}$. It can be seen that for all flow rates, the copper tube has a lower $S_{g,tot}$ than the steel one.

In Fig. 7, the amounts of Ex_{out} are presented for the blade, brick, platelet, and cylinder-shaped NPs with different values of ϕ for copper and steel collectors. It can be seen that the changes in the graphs are the same for the two types of tubes. In both tubes, except for the brick-shaped NPs, an increment in the amount of NPs reduces and then enhances the amount of Ex_{out}. Adding NPs reduces the heat capacity of the fluid but intensifies the temperature at the output, leading to the changes in the Ex_{out} with ϕ. The NFs flowing in the copper tube has more exergy than the NFs moving the steel tube. Ex_{out} of copper tube is higher than that of steel one.

Fig. 8 demonstrates Ex_{loss} for the blade, brick, platelet, and cylinder-shaped NPs with different values of ϕ for copper and steel collectors. The variations of Ex_{loss} are the same as Ex_{out} for different shapes of NPs. However, the initial reduction in Ex_{loss} at $\phi = 1\%$ is greater than Ex_{out}. It can be seen that the amount of Ex_{loss} in the copper tube is higher than that in steel one. Platelet-shaped NPs have the minimum Ex_{loss} and Brick-shaped ones have the maximum Ex_{loss} when $\phi = 4\%$.

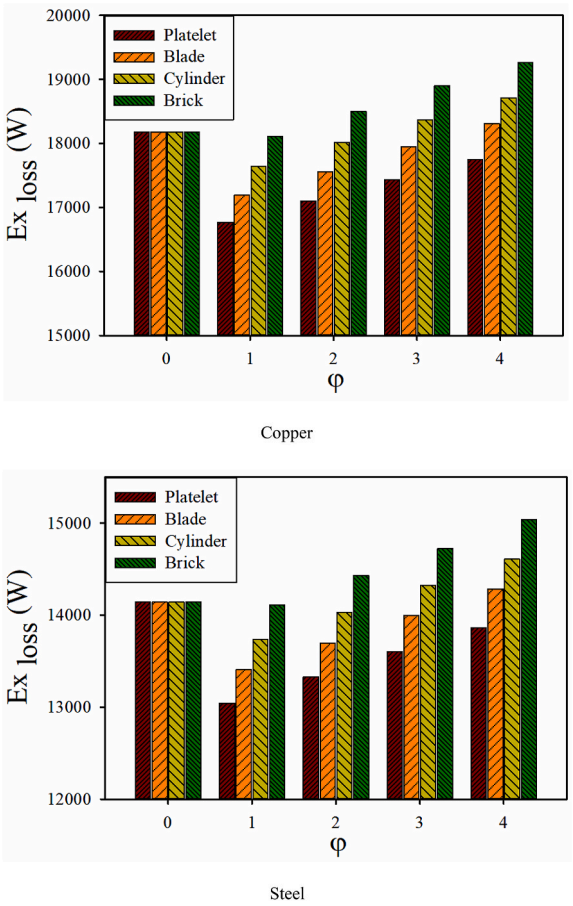

Fig. 8. Ex_{loss} for the blade, brick, platelet, and cylinder-shaped NPs with different values of ϕ for copper and steel collectors.

5. Conclusions

In this paper, the second-law analysis of boehmite alumina/water-ethylene glycol (50:50) NFs flow is performed for a SC with a hexagonal cross section. $S_{g,ff}$, $S_{g,th}$, $S_{g,tot}$, Ex_{out}, and Ex_{loss} are analyzed for copper and steel tubes by changing the flow rate and volume percentage of the blade, cylinder, platelet, and brick-shaped NPs. The results of this study demonstrate:

1 An increment in ϕ up to 1% for the blade, cylinder, and platelet-shaped NPs reduce the amount of $S_{g,ff}$, but further enhancement of the percentage of NPs intensifies these values.
2 Ex_{out} and Ex_{loss} in the copper tube are higher than those in steel one. The values of $S_{g,th}$, and $S_{g,tot}$ for steel tube are higher than those for copper tube.
3 Platelet-shaped NPs have the maximum value of $S_{g,tot}$, and the minimum Ex_{out} is obtained for these NPs.
4 The addition of NPs to ethylene glycol enhances $S_{g,ff}$ and reduces $S_{g,th}$ when $\phi = 4\%$. Platelet and cylinder-shaped NPs enhance $S_{g,tot}$ at a high value of ϕ, but the blade and brick-shaped NPs reduce $S_{g,tot}$.
5 An increment in the NFs flow rate in both tubes enhances the amount of $S_{g,tot}$. For platelet shape, by increasing the mass flow rate from 0.25 to 1 kg/s, nanoparticles in steel and copper collectors increase the total production entropy by 7.9 and 8.4 times, respectively.

Authors' contributions

Abdullah K. Alanazi: Funding acquisition; Writing - original draft. Yacine Khetib: Formal analysis; Writing - review & editing. Hala M. Abo-Dief: Writing - review & editing. Muhyaddin Rawa: Writing - review & editing. Goshtasp Cheraghian: Conceptualization; Review & editing. Mohsen Sharifpur: Conceptualization.

Declaration of competing interest

The authors declare that they have no known competing financial interests or personal relationships that could have appeared to influence the work reported in this paper.

Acknowledgements

This work was supported by the Taif University Researchers Supporting grant number (TURSP-2020/266) of Taif University, Taif, Saudi Arabia.

References

[1] C. Lamnatou, D. Chemisana, Photovoltaic/thermal (PVT) systems: a review with emphasis on environmental issues, Renew. Energy 105 (2017/05/01/2017) 270–287.
[2] H. Caliskan, Energy, exergy, environmental, enviroeconomic, exergoenvironmental (EXEN) and exergoenviroeconomic (EXENEC) analyses of solar collectors, Renew. Sustain. Energy Rev. 69 (2017/03/01/2017) 488–492.
[3] A. Geete, A. Bhattacharjee, A. Patwa, K. Pandey, Entropy, exergy and entransy analyses on fabricated shell and spiral tube heat exchanger, J. Inst. Eng.: Series C 102 (4) (2021/08/01 2021) 897–908.
[4] A. Geete, V. Patel, S.S. Tanwar, S. Kushwah, N.S. Lodhi, V. Kushwah, Thermodynamic analysis of designed and fabricated shell- and tube-type heat exchanger by DSTHE software: kern method, Int. J. Ambient Energy 39 (4) (2018/05/19 2018) 343–351.
[5] A. Geete, A. Dubey, A. Sharma, A. Dubey, Exergy analyses of fabricated compound parabolic solar collector with evacuated tubes at different operating conditions: indore (India), J. Inst. Eng.: Series C 100 (2019) 455–460.
[6] W.S. Sarsam, S.N. Kazi, A. Badarudin, A review of studies on using nanofluids in flat-plate solar collectors, Sol. Energy 122 (2015/12/01/2015) 1245–1265.
[7] L. Evangelisti, R. De Lieto Vollaro, F. Asdrubali, Latest advances on solar thermal collectors: a comprehensive review, Renew. Sustain. Energy Rev. 114 (2019/10 2019) 109318.
[8] A.K. Hussein, Applications of nanotechnology to improve the performance of solar collectors – recent advances and overview, Renew. Sustain. Energy Rev. 62 (2016/09/01/2016) 767–792.
[9] G. Yu, C. Du, H. Chen, L. Xiong, A dynamic model based on response factor method and seasonal performance analysis for integration of flat plate solar collector with building envelope, Appl. Therm. Eng. 150 (2019/03 2019) 316–328.
[10] S.-R. Yan, A. Golzar, M. Sharifpur, J.P. Meyer, D.-H. Liu, M. Afrand, Effect of U-shaped absorber tube on thermal-hydraulic performance and efficiency of two-fluid parabolic solar collector containing two-phase hybrid non-Newtonian nanofluids, Int. J. Mech. Sci. 185 (2020/11/01/2020) 105832.
[11] M.M. Thalib, M. Vimala, A.M. Manokar, R. Sathyamurthy, M. Sadeghzadeh, M. Sharifpur, Energy, exergy and economic investigation of passive and active inclined solar still: experimental study, J. Therm. Anal. Calorim. 145 (3) (2021/08/01 2021) 1091–1102.
[12] M.E.H. Attia, A. Karthick, A.M. Manokar, Z. Driss, A.E. Kabeel, R. Sathyamurthy, M. Sharifpur, Sustainable potable water production from conventional solar still during the winter season at Algerian dry areas: energy and exergy analysis, J. Therm. Anal. Calorim. 145 (No. 3) (2021/08/01, 2021) 1215–1225.
[13] A. Allouhi, M. Benzakour Amine, M.S. Buker, T. Kousksou, A. Jamil, Forced-circulation solar water heating system using heat tube-flat plate collectors: energy and exergy analysis, Energy 180 (2019/08/01/2019) 429–443.
[14] Y. Hu, J.X. Qing, Z.H. Liu, Z.J. Conrad, J.N. Cao, X.P. Zhang, Hovering efficiency optimization of the ducted propeller with weight penalty taken into account, Aero. Sci. Technol. 117 (2021), https://doi.org/10.1016/j.ast.2021.106937.
[15] G.X. Xiang, X. Gao, W.J. Tang, X.Z. Jie, X. Huang, Numerical study on transition structures of oblique detonations with expansion wave from finite-length cowl, Phys. Fluids 32 (5) (2020) 56108, https://doi.org/10.1063/5.0005189.
[16] Y. Du, N. Pan, Z. Xu, F. Deng, Y. Shen, H. Kang, Pavement distress detection and classification based on YOLO network, Int. J. Pavement Eng. (2020) 1–14, https://doi.org/10.1080/10298436.2020.1714047.
[17] Z. Lu, L. Zhao, H. Ding, L. Chen, A dual-functional metamaterial for integrated vibration isolation and energy harvesting, J. Sound Vib. 509 (2021) 116251, https://doi.org/10.1016/j.jsv.2021.116251.
[18] X. Li, X. Sheng, Y. Guo, X. Lu, H. Wu, Y. Chen, J. Gu, Multifunctional HDPE/CNTs/PW composite phase change materials with excellent thermal and electrical conductivities, J. Mater. Sci. Technol. 86 (2021) 171–179, https://doi.org/10.1016/j.jmst.2021.02.009.
[19] E. Farajzadeh, S. Movahed, R. Hosseini, Experimental and numerical investigations on the effect of Al_2O_3/TiO_2H_2O nanofluids on thermal efficiency of the flat plate solar collector, Renew. Energy 118 (2018/04 2018) 122–130.
[20] J. Mustafa, S. Alqaed, R. Kalbasi, Challenging of using CuO nanoparticles in a flat plate solar collector- Energy saving in a solar-assisted hot process stream, J. Taiwan Inst. Chem. Eng. 124 (2021/07/01/2021) 258–265.
[21] W. Hao, Y. Lu, Y. Lai, H. Yu, M. Lyu, Research on operation strategy and performance prediction of flat plate solar collector with dual-function for drying agricultural products, Renew. Energy 127 (2018/11/01/2018) 685–696.
[22] H. Kaya, K. Arslan, N. Eltugral, Experimental investigation of thermal performance of an evacuated U-Tube solar collector with ZnO/Etylene glycol-pure water nanofluids, Renew. Energy 122 (2018/07/01/2018) 329–338.
[23] A. Hajatzadeh Pordanjani, S. Aghakhani, M. Afrand, B. Mahmoudi, O. Mahian, S. Wongwises, An updated review on application of nanofluids in heat exchangers for saving energy, Energy Convers. Manag. 198 (2019/10/15/2019) 111886.
[24] S.-R. Yan, S. Aghakhani, A. Karimipour, Influence of a membrane on nanofluid heat transfer and irreversibilities inside a cavity with two constant-temperature semicircular sources on the lower wall: applicable to solar collectors, Phys. Scripta 95 (8) (2020), 085702.
[25] S.-R. Yan, A. Hajatzadeh Pordanjani, S. Aghakhani, A. Shahsavar Goldanlou, M. Afrand, Managment of natural convection of nanofluids inside a square enclosure by different nano powder shapes in presence of Fins with different shapes and magnetic field effect, Adv. Powder Technol. 31 (2020/07/01/2020) 2759–2777.
[26] S.U. Choi, J.A. Eastman, Enhancing Thermal Conductivity of Fluids with Nanoparticles, Argonne National Lab., IL (United States), 1995.
[27] S. Aghakhani, B. Ghasemi, A. Hajatzadeh Pordanjani, S. Wongwises, M. Afrand, Effect of replacing nanofluid instead of water on heat transfer in a channel with extended surfaces under a magnetic field, Int. J. Numer. Methods Heat Fluid Flow 29 (4) (2019) 1249–1271.
[28] S. Aghakhani, A.H. Pordanjani, M. Afrand, M. Sharifpur, J.P. Meyer, Natural convective heat transfer and entropy generation of alumina/water nanofluid in a tilted enclosure with an elliptic constant temperature: applying magnetic field and radiation effects, Int. J. Mech. Sci. 174 (2020/05/15/2020) 105470.
[29] A.H. Pordanjani, S. Aghakhani, Numerical investigation of natural convection and irreversibilities between two inclined concentric cylinders in presence of uniform magnetic field and radiation, Heat Tran. Eng. (2021) 1–21.
[30] G. Cheraghian, Improved heavy oil recovery by nanofluid surfactant flooding-an experimental study, Eur. Assoc. Geosci. & Eng. 2016 (2016) 1–5, https://doi.org/10.3997/2214-4609.201601509.
[31] G. Cheraghian, S.S. Khalili Nezhad, S. Bazgir, Improvement of thermal stability of polyacryl amide solution used as a nano-fluid in enhanced oil recovery process by nanoclay, Int. J. Nanosci. Nanotechnol. 11 (2015) 201–208.
[32] M.-W. Tian, S. Rostami, S. Aghakhani, A.S. Goldanlou, C. Qi, Investigation of 2D and 3D configurations of fins and their effects on heat sink efficiency of MHD hybrid nanofluid with slip and non-slip flow, Int. J. Mech. Sci. (2020/07/25/2020) 105975.

[33] S.O. Giwa, M. Sharifpur, J.P. Meyer, S. Wongwises, O. Mahian, Experimental measurement of viscosity and electrical conductivity of water-based γ-Al2O3/MWCNT hybrid nanofluids with various particle mass ratios, J. Therm. Anal. Calorim. 143 (2) (2021/01/01 2021) 1037–1050.
[34] X. Zhang, X. Sun, T. Lv, L. Weng, M. Chi, J. Shi, S. Zhang, Preparation of PI porous fiber membrane for recovering oil-paper insulation structure, J. Mater. Sci. Mater. Electron. 31 (16) (2020) 13344–13351, https://doi.org/10.1007/s10854-020-03888-5.
[35] X. Li, Y. Feng, B. Liu, D. Yi, X. Yang, W. Zhang, P. Bai, Influence of NbC particles on microstructure and mechanical properties of AlCoCrFeNi high-entropy alloy coatings prepared by laser cladding, J. Alloys Compd. 788 (2019) 485–494, https://doi.org/10.1016/j.jallcom.2019.02.223.
[36] S. Yang, X. Wan, K. Wei, W. Ma, Z. Wang, Silicon recovery from diamond wire saw silicon powder waste with hydrochloric acid pretreatment: an investigation of Al dissolution behavior, Waste Manag. 120 (2021) 820–827, https://doi.org/10.1016/j.wasman.2020.11.005.
[37] M. Hatami, S. Mosayebidorcheh, D. Jing, Thermal performance evaluation of alumina-water nanofluid in an inclined direct absorption solar collector (IDASC) using numerical method, J. Mol. Liq. 231 (2017/04/01/2017) 632–639.
[38] H. Khakrah, A. Shamloo, S. Kazemzadeh Hannani, Exergy analysis of parabolic trough solar collectors using Al_2O_3/synthetic oil nanofluid, Sol. Energy 173 (2018/10/01/2018) 1236–1247.
[39] M. Khoshvaght-Aliabadi, M. Tatari, M. Salami, Analysis on Al_2O_3/water nanofluid flow in a channel by inserting corrugated/perforated fins for solar heating heat exchangers, Renew. Energy 115 (2018/01/01/2018) 1099–1108.
[40] I.M. Mahbubul, M.M.A. Khan, N.I. Ibrahim, H.M. Ali, F.A. Al-Sulaiman, R. Saidur, Carbon nanotube nanofluid in enhancing the efficiency of evacuated tube solar collector, Renew. Energy 121 (2018/06/01/2018) 36–44.
[41] O.Z. Sharaf, D.C. Kyritsis, E. Abu-Nada, Impact of nanofluids, radiation spectrum, and hydrodynamics on the performance of direct absorption solar collectors, Energy Convers. Manag. 156 (2018/01/15/2018) 706–722.
[42] M. Siavashi, K. Ghasemi, R. Yousofvand, S. Derakhshan, Computational analysis of SWCNH nanofluid-based direct absorption solar collector with a metal sheet, Sol. Energy 170 (2018/08/01/2018) 252–262.
[43] E. Shahsavani, M. Afrand, R. Kalbasi, Using experimental data to estimate the heat transfer and pressure drop of non-Newtonian nanofluid flow through a circular tube: applicable for use in heat exchangers, Appl. Therm. Eng. 129 (2018/01/25/2018) 1573–1581.
[44] S.A. Mirmohammadi, M. Behi, Y. Gan, L.J.P.R.E. Shen, Particle-shape-, Temperature-, and Concentration-dependent Thermal Conductivity and Viscosity of Nanofluids, vol. 99, 2019, 043109.
[45] S. Sadripour, A.J. Chamkha, The effect of nanoparticle morphology on heat transfer and entropy generation of supported nanofluids in a heat sink solar collector, Thermal Sci. Eng. Progr. 9 (2019/03/01/2019) 266–280.
[46] S.M. Vanaki, H.A. Mohammed, A. Abdollahi, M.A. Wahid, Effect of nanoparticle shapes on the heat transfer enhancement in a wavy channel with different phase shifts, J. Mol. Liq. 196 (2014/08/01/2014) 32–42.
[47] A.A.A. Arani, S. Sadripour, S. Kermani, Nanoparticle shape effects on thermal-hydraulic performance of boehmite alumina nanofluids in a sinusoidal–wavy mini-channel with phase shift and variable wavelength, Int. J. Mech. Sci. 128–129 (2017/08/01/2017) 550–563.
[48] S.A. Kalogirou, Solar Energy Engineering: Processes and Systems, Academic Press, 2013.
[49] V. Gnielinski, New equations for heat and mass transfer in turbulent tube and channel flow, Int. Chem. Eng. 16 (1976) 359–368.
[50] C.F. Colebrook, T. Blench, H. Chatley, E. Essex, J. Finniecome, G. Lacey, et al., Correspondence. turbulent flow in tubes, with particular reference to the transition region between the smooth and rough tube laws.(includes plates), J. Inst. Civil Eng. 12 (1939) 393–422.
[51] A. Bejan, Entropy Generation through Heat and Fluid Flow, vol. 1, Wiley, New York, 1982.
[52] K. Dutta Gupta, S.K. Saha, Energy analysis of solar thermal collectors, Renewable Energy Environ. 5 (1990) 283–287.
[53] S. Farahat, F. Sarhaddi, H. Ajam, Exergetic optimization of flat plate solar collectors, Renew. Energy 34 (2009/04/01/2009) 1169–1174.
[54] A. Suzuki, General theory of exergy-balance analysis and application to solar collectors, Energy 13 (1988/02/01/1988) 153–160.
[55] Y.A. Çengel, J.M. Cimbala, Fluid Mechanics: Fundamentals and Applications, McGraw-Hill Higher Education, 2010.
[56] S.S. Khaleduzzaman, M.R. Sohel, I.M. Mahbubul, R. Saidur, J. Selvaraj, Exergy and entropy generation analysis of TiO2–water nanofluid flow through the water block as an electronics device, Int. J. Heat Mass Tran. 101 (2016/10/01/2016) 104–111.
[57] E.V. Timofeeva, J.L. Routbort, D. Singh, Particle shape effects on thermophysical properties of alumina nanofluids, J. Appl. Phys. 106 (2009), 014304.